RSC Advances

ROYAL SOCIETY OF CHEMISTRY

www.rsc.org/advances

Effects of extrusion draw ratio on morphology, structure and mechanical properties of poly(L-lactic acid) fabricated by solid state ram extrusion

Hua-Mo Yin, Huan Xu, Jin Zhang, Jing-Bin Chen, Jun Lei, Jia-Zhuang Xu* and Zhong-Ming Li*

College of Polymer Science and Engineering and State Key Laboratory of Polymer Materials Engineering, Sichuan University, Chengdu 610065, China

*Corresponding author. Tel.: +86-28-8540-0211; Fax: +86-28-8540-5402; E-mail address: zmli@scu.edu.cn (Z.M. Li); E-mail address: jzxu@scu.edu.cn (J.Z. Xu)

Abstract:

Solid state ram extrusion (SSRE) was utilized to fabricate poly(L-lactic acid) (PLLA) and effects of extrusion draw ratios (EDRs) on its morphology, structure, and properties were investigated. Scanning electron microscopy observation indicated that the original spherulites gradually transformed into microfibrils aligned along the extrusion direction with the increase of EDR. The molecular orientation of SSRE PLLA proceeded with EDR in both sheath and core region as detected by wide-angle X-ray diffraction (WAXD) and small-angle X-ray scattering characterizations. Interestingly, on the basis of WAXD diffraction curves, the β form of PLLA was found to appear in the bulk extrudates when EDR was beyond 4.0, where the crystal transformation from the premier α to β form occurred between $(203)_{\alpha}$ and $(131)_{\beta}$. Meanwhile, the sheath region contained much higher amount of β form than the core region, contributing to the existence of larger deformation in the sheath region. A multiple melting phenomenon of PLLA consisting of α and β mixture crystals was revealed by on-line WAXD and differential scanning calorimetry (DSC) measurement, which was explained by the melting, recrystallization and remelting. Formation of the fibrous crystals and melting re-crystallization may lead to the increase of the melting point of SSRE PLLA. Additionally, flexural strength and flexural modulus showed monotonous rise with EDR, achieving 4 and 13 times higher for the specimen at the EDR of 8.2 relative to the sample at the EDR of 1.0, respectively.

1. Introduction

Taking the merits such as absorbability, renewability, degradability to nontoxic products, no tissue reaction and no second removal operation into account, poly(L-lactic acid) (PLLA) has been introduced to the biomedical application, such as orthopedic, craniofacial and oral-maxillofacial bone fixation.[1-5] Unfortunately, the inferior mechanical properties of PLLA, such as low ductility and low strength,[6] make it difficult to match the bone tissues that may endure high loading, *i.e.*, thighbone, becoming an obstacle for preferable internal bone fixation. Therefore, it is of importance to improve mechanical properties of PLLA.

As is well established, mechanical properties of a crystalline polymer rest upon its hierarchical structures strongly,[7, 8] especially the crystalline structures. It has been recognized that PLLA mainly has four crystalline modifications (α, β, γ, and α') relying on the crystallization conditions. The most common polymorph is α form with typical 10_3 helical chain conformation.[9-12] which grows upon normal melt or solution crystallization.[13, 14] Drawing the PLLA fibers near melting point induces the β form, which also possesses 3_1 helical chain conformation.[10, 15] By epitaxially crystallizing on hexamethylbenzene, the γ form of PLLA was obtained and had a 3_2 helical chain conformation.[16] A new modification of PLLA named the α' form was subsequently observed by Zhang *et al.* at the isothermal crystallization temperature below 120 °C. They proposed that the α' form with a loose 10_3 helical chain conformation was a type of the frustrated α form and less thermally stable than the normal α form.[17]

Although different crystalline modifications of PLLA are already obtained via

controlling the explicit experiment conditions, it has not yet been realized to fabricate the certain crystalline modification and structure of PLLA in the practical processing, especially for the β form. Relationship between its crystalline structure and mechanical property has, thus, rarely been reported. By surveying the existing literatures, we found that the β form mainly forms in PLLA fibers prepared either by melt spinning or by solution spinning. For instance, Eling *et al.*[9] reported that high temperature and large draw ratio were beneficial to inducing the β form of PLLA, while α form of PLLA was gained at low temperature and at low draw ratio. Leenslag *et al.*[18] found an α-β crystal transition in PLLA fibers produced by dry spinning and subsequently hot drawing. In addition, by controlling the processing conditions of solution spinning, including high draw temperature (200 ~ 204 °C), ultra-large draw ratio (14 ~ 20), high molecular weight (5.6 ~ 9 × 10^5), and molecular weight distribution, Hoogsteen *et al.*[19] obtained the PLLA fibers that only consisted of β form. Nevertheless, the utilization of PLLA fibers containing the β form was restricted due to the diminutive cross sections. And fabrication of the bulk PLLA products with the β form is still a big challenge till now.

Solid state extrusion (SSE) has become a widely applied technology since the 1970s, which falls into two major types, that is, solid state hydrostatic extrusion (SSHE) and solid state ram extrusion (SSRE).[20-25] Strong deformation of polymeric billets occurred during the SSHE and SSRE, inducing the molecular chain orientation, crystal fragmentation, distortion, recrystallization, fibrillation, and so forth. It is exactly because of the above structural evolution, the extrudates usually exhibit

superior mechanical properties. Gogolewski *et al.*[26] successfully prepared the SSE PLLA with a yield flexural strength of 215 MPa and a modulus of 13.7 GPa, which respectively presented 67% and 204% increment compared to the melt-extruded PLLA. On the other hand, SSE held great potential for fabricating the bulk material containing β form because of the intense complex fields existed, such as shear and extensional field. Sawai *et al.*[27] observed that with the increase of EDR in SSE, the isotropic α form of PLLA gradually transformed into the oriented β form, where only β crystals were observed near the maximum EDR of 11. As detected by wide-angle X-ray diffraction (WAXD), it was confirmed that there was a transformation between $(003)_\beta$ and $(0010)_\alpha$. Their further work reported the transition from α into β form was influenced by many factors, such as extrusion temperature, pressure, molecular weight, and EDR.[28, 29] However, despite all this, the formation condition of β crystals in the SSRE is still a little elusive, such as the necessity of rigorous conditions and the lattice plane of crystal transformation.

In the present study, we aimed at exploring the influence of EDRs on the oriented morphology, crystalline structure, and flexural properties of bulk PLLA fabricated by the SSRE technique. It was found that a large amount of highly oriented microfibrils was observed in the SSRE PLLA along the extruded direction. Molecular orientation presented monotonically ascending tendency with the increase of EDR. Rather interestingly, β crystals appeared when EDR exceeded 4.0, where the crystal transformation was suggested to happen between $(203)_\alpha$ and $(131)_\beta$. And more β form existed in the sheath than the core. The melting, recrystallization and remelting

process gave a reasonable explanation for the hierarchical melting behavior of the SSRE PLLA. Furthermore, both flexural strength and flexural modulus showed prominent enhancement with EDR, reaching 4 and 13 times higher for the specimen at the EDR of 8.2 in comparison with the sample at the EDR of 1.0, respectively.

2. Materials and methods

2.1 Materials

Commercially available PLLA (trade name 4032D) was purchased from NatureWorks, whose weight-average molecular weight and polydispersity index were 2.23×10^5 g/mol and 1.6, respectively.

2.2 Solid-State Extrusion

The home-made SSRE apparatus as schematically shown in Fig. 1a was employed to prepare the PLLA rods. The raw material was first dried in a vacuum oven for 24 h at 100 ℃ and stored in a desiccator prior to processing. Temperature protocol of the SSRE was presented in Fig. 1b. Cylindrical billets with diameter of 20 mm were prepared at 190 ℃ for 30 min by the compression molding in the SSRE apparatus. The SSRE of PLLA was performed by pulling the as-prepared billet through the die at a constant temperature (155 ℃), which was an optimum extrusion temperature after multiple trials. It should be emphasized that the drawing rate during the extrusion is so slow to guarantee the sufficient time for the deformation of PLLA billets. The EDR is defined as the cross-sectional area ratio of initial billet to the final extrudate, that is

to say, the EDR increased with the decrease of the diameter of conical die. By calculation, the EDRs of PLLA rods prepared in this study were 1.0, 4.0, 6.3, and 8.2. The SSRE specimens with different EDRs were successfully obtained eventually. Fig. 1c represents a segment of the specimen with an EDR of 8.2.

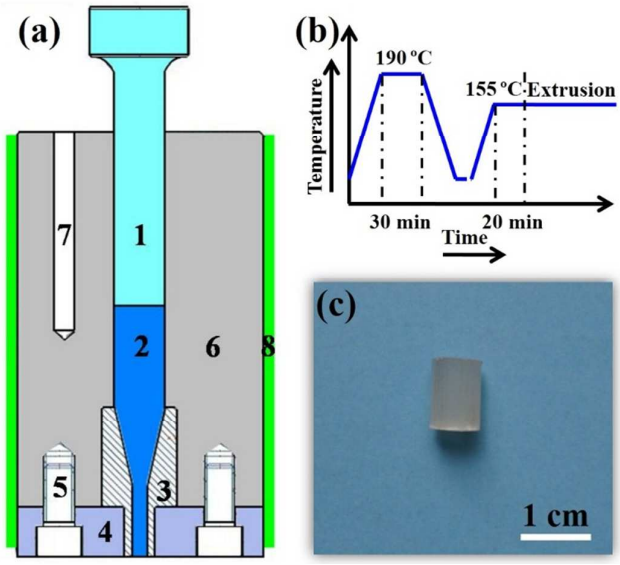

Fig. 1 (a) Schematic of the SSRE apparatus (1: piston; 2: billet; 3: die; 4: fixed plate; 5: screw; 6: barrel; 7: thermocouple; 8: heater circle); (b) schematic diagram of the temperature protocol; (c) digital photo of segmental SSRE PLLA with an EDR of 8.2.

2.3 Scanning Electron Microscopy (SEM)

The PLLA extrudates were frozen in liquid nitrogen for about 20 min and were split longitudinally. Prior to SEM observation, the cryogenically fractured surface of samples were sprayed with a thin golden coating. The morphology of PLLA extrudates was investigated by utilizing a field emission SEM (Inspect F, FEI, Finland) at an accelerated voltage of 20 kV. Each PLLA extrudate was divided into two regions, namely sheath and core. Herein, the sheath was defined as the layer from the surface

to 1 mm inside, and the cylinder with the width of 1 mm located in the center of the extrudate was named as the core. SEM observation examined severally in these two regions.

2.4 Synchrotron Wide-Angle X-ray Diffraction (WAXD)

WAXD measurement was carried out at the beamline BL16B1 of Shanghai Synchrotron Radiation Facility (SSRF, Shanghai, China). The monochromatic X-ray beam with a wavelength of 0.124 nm was focused to an area of 80 μm × 80 μm (length × width) and the distance from sample to detector was 109.5 mm. Two-dimensional WAXD (2D-WAXD) images were collected with an X-ray CCD detector. The samples for WAXD measurement were obtained by splitting along the axial direction of extrudates and machined into one flake with the thickness of 1 mm. The flake was scanned from the sheath to the core at a step of 500 μm. Fit-2D software package was used to analyze the 2D-WAXD patterns, and linear WAXD profiles were obtained by circularly integrating the intensities of 2D-WAXD patterns acquired. The 2θ angles of samples were corrected by the function $q = 4\pi \sin \theta_1/\lambda_1 = 4\pi \sin \theta_2/\lambda_2$, where the first-order scattering vector (q) is a constant, λ_1 (0.124 nm) and λ_2 (0.154 nm) are the typical wavelengths of experimental beamline and common Cu Kα radiation, respectively. The melting process of the SSRE extrudate was also detected, the temperature profile of which was controlled by a Linkam hot stage. The sheath of the SSRE extrudate with the EDR of 8.2 was placed in the gap of hot stage. The sample was heated from 100 to 200 °C at a constant rate of 10 °C/min, and the

data acquisition time was 3 s for each scattering pattern.

2.5 Synchrotron Small-Angle X-ray Scattering (SAXS)

To investigate the interior structure of extrudates, SAXS measurement was performed using the beamline BL16B1 at Shanghai Synchrotron Radiation Facility (SSRF, Shanghai, China). The wavelength of monochromatic X-ray beam was 0.124 nm with a beam size of 80 μm × 80 μm (length × width), and the distance from sample to detector was held at 2010 mm. An X-ray CCD detector was employed for detecting the 2D-SAXS images. The samples for SAXS measurement were the same as those for WAXD measurement. The long period on behalf of the thickness between the adjacent lamellae is calculated by using the Bragg equation, $L = 2\pi/q^*$, where L is long period and q^* stands for the peak position in the scattering curves.

2.6 Differential Scanning Calorimetry (DSC)

The melting behavior of SSRE extrudates was measured by a TA-Q2000 DSC (TA Instruments, USA). The samples for DSC measurement were taken from the sheath and the core of SSRE PLLA with different EDR, respectively. The samples (about 5 ~ 7 mg) were heated from 40 to 190 ℃ at a rate of 10 ℃/min under nitrogen atmosphere. Melting point (T_m) and melting enthalpy (ΔH_m) were determined from the temperature and area of endothermic peak, respectively. Crystallinity (X_c) was calculated by

$$X_c = \frac{\Delta H_m - \Delta H_{cc}}{\Delta H_0} \times 100\% \quad (1)$$

where ΔH_m is the melting enthalpy, ΔH_{cc} represents the cold crystalline enthalpy, ΔH_0 is the melting enthalpy of 100% crystalline PLLA. For $X_{c\,\alpha}$, $\Delta H_{0\,\alpha}$ is taken as 93.7 J/g, while $\Delta H_{0\,\beta}$ is set as 124 J/g for $X_{c\,\beta}$ in this study.[27, 30]

2.7 Mechanical Properties

Three point flexural tests were performed at ambient temperature using an Instron testing machine (Model 4302, Instron Instruments, USA) with a crosshead speed of 1 mm min^{-1} and a 10 kN load cell. The span length (L) was regulated at 28 mm. The extrudates with different EDRs were cut into cylinders with the length of 36 mm along the extrusion direction and were tested ($n \geq 4$) at each EDR. Flexural strength and flexural modulus were calculated from following Equations:

$$\text{Flexural strength} = \frac{8F_{max}L}{\pi d^3} \quad (2)$$

$$\text{Flexural modulus} = \frac{4L^4}{3\pi d^3} \bullet \frac{E}{Y} \quad (3)$$

where F_{max} is the maximum force and d is diameter of the sample. E/Y is the linear gradient of the load-displacement curve.

3. Results and discussion

3.1 Morphological Observation of the SSRE PLLA Extrudates

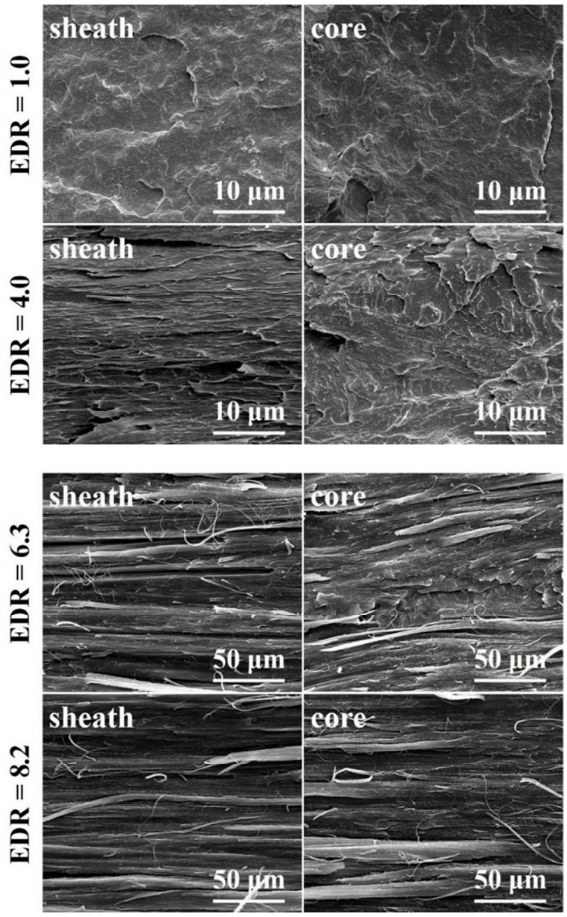

Fig. 2 SEM images of the split surface of the SSRE PLLA with different EDRs.

To determine the morphological evolution of SSRE PLLA extrudates with EDR, SEM characterization was performed on the sheath and core region of each specimen, respectively, as presented in Fig. 2. At the EDR of 1.0, smooth fractured surface was observed in both sheath and core, showing typical brittle fracture feature and isotropic state of crystals in the billet prior to extrusion. With the EDR increasing, the dense array of microfibrillar structure in the PLLA extrudates appears, which results from deformation and orientation of crystallites by the imposed complex flow fields during SSRE. The morphology and size of the microfibrils are greatly affected by the EDR.

To be specific, at the EDR of 4.0, regular framework of ribbon-like fibrillar structure already forms in the sheath, while the irregular orientation of layer-like structure is still dominated in the core. As the EDR further increases, robust microfibrils appear in both sheath and core. The microfibrils in the sheath seem to show strong orientation along the extrusion direction compared to those in the core until the EDR reaches 8.2, suggesting that there is a gradient distribution of the shear force imposed from the sheath to the core. At the higher EDR, the fibrillar structures become neater due to the stronger shear force. The reason for the morphology transformation of PLLA extrudates is closely related to the distortion and fragmentation of spherulites, accompanying with lamellae orientation, slippage and rearrangement into fibrillation along the extrusion direction. The fibrillations of PLLA occurred at higher EDR could be considered as a self-reinforcement structure, which advances in the final mechanical properties of PLLA.[26]

3.2 WAXD Analysis of the SSRE PLLA Extrudates

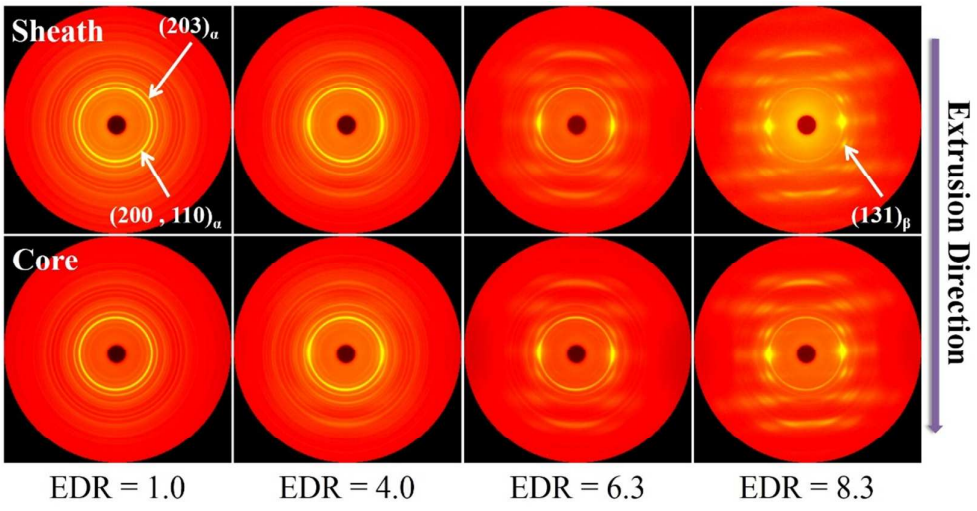

Fig. 3 Typical 2D-WAXD images of SSRE PLLA rods at different EDRs.

Fig. 3 illustrates the typical 2D-WAXD patterns to further acquire the specific structural information on the microfibrils of SSRE PLLA extrudates. Isotropic diffraction rings represented the α form of PLLA, *i.e.*, $(200)_\alpha$ and $(110)_\alpha$ reflections are clearly observed in the sheath and core of PLLA extrudate with EDR of 1.0, indicating PLLA lamellae present a random distribution in the bulk. Inversely, visible arc-like diffractions appear in the equator direction, and the diffraction intensities gradually become stronger as the EDR increases. The isotropic diffraction rings almost disappear and only the reflection arcs are present in the equator for both the sheath and core of PLLA extrudates at the EDR of 8.2. It confirms that the molecular chains preferentially arrange along the extrusion direction, mainly resulting from the large deformation force provided by SSRE process. Apparently, the variation tendency of the diffraction features in the core is similar to that of the sheath, as observed in Fig. 3. It should be noted that small amounts of oriented β crystals are appreciably detected in the WAXD patterns at the EDR of 6.3 and 8.2, indicating the transformation from primitive α crystals transform to β crystals. The details of crystal transformation will be further discussed later.

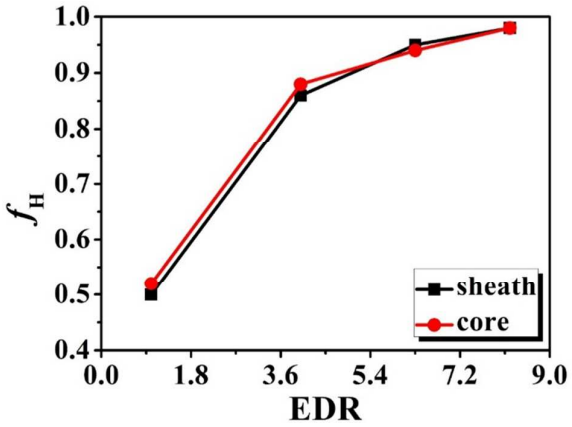

Fig. 4 Orientation functions f_H for the sheath and the core regions of SSRE PLLA rods for different EDRs, calculated from the $(200)_\alpha$ and $(110)_\alpha$ reflection.

To quantitatively evaluate the degree of orientation, the orientation function (f_H) of PLLA extrudates was calculated from the $(200)_\alpha/(110)_\alpha$ reflection along the azimuthal angle. As presented in Fig. 4, the f_H of SSRE PLLA extrudates exhibits monotonically climbing tendency with EDR, reaching very high orientation at the EDR of 8.2 (f_H = 0.98). The high degree of orientation is well consistent with the SEM result. It manifests that the SSRE technique could induce highly oriented PLLA lamellae, which is attributed to the fact that the intense flow field in the die compels the rearrangement and orientation of molecular chains. Remarkably, in comparison with the f_H value of extrudates by solid state coextrusion once reported,[28] it should be addressed that utilization of SSRE in our present study requires smaller EDR to make the bulk PLLA reach such a high orientation. Beyond this, there is almost no difference of the f_H between the sheath and the core of PLLA extrudates at the EDR higher than 6, implying the bulk material is relatively homogeneous. And the uniform

inner structure is preferable to ameliorate the mechanical performance of PLLA materials.

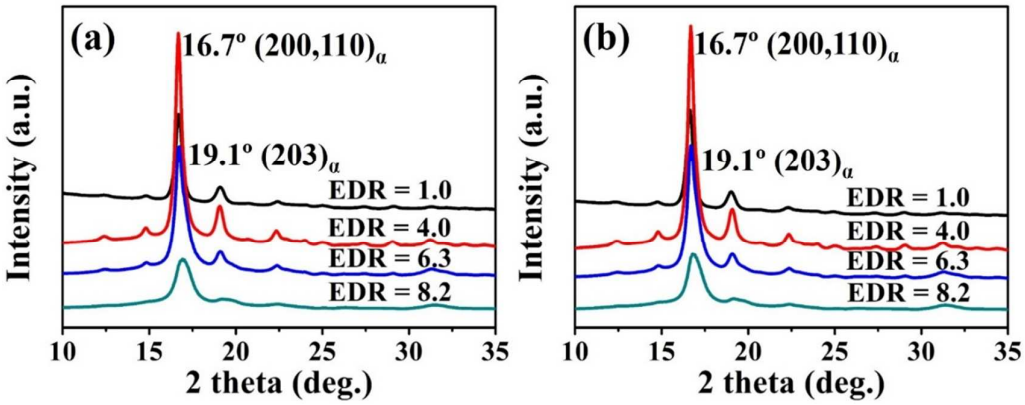

Fig. 5 Representative 1D-WAXD curves of SSRE PLLA rods at different EDRs: (a) sheath, (b) core.

Fig. 5 shows the corresponding 1D-WAXD curves of PLLA samples at different EDRs circularly integrated the 2D-WAXD patterns in Fig. 3. It could be identified that there are two strong diffraction peaks at 2θ = 16.7° and 19.2°, indicative of lattice planes (200)/(110) and (203) reflections of the α-form crystal, respectively. In the sheath, the diffraction intensities of PLLA extrudates are relatively strong at the low EDR and gradually transform into almost the baby-size diffraction peak with the increase of EDR, elucidating that the crystallinity of extrudates reduces with the EDR. As for the core, the similar variation tendency is observed. Note that the intensity of $(203)_\alpha$ reflection weakens accompanied by the peak shifting to a higher value.

The magnified 1D-WAXD curves of SSRE PLLA in the range of 2θ from 18° to 24° is highlighted in Fig. 6. Upon extrusion to the high EDR, the keen-edge diffraction peak is replaced by the flat diffraction peak. More interestingly, a weak peak at 2θ =

19.6º close to the main peak rises up slowly. The new emerging peak in the sheath and the core stands for the $(131)_\beta$ reflection of PLLA β crystals. The increase in the intensity of the $(131)_\beta$ reflection is accompanied by the shifting of $(203)_\alpha$ reflection to a low value, implicating the conversion of the initial α form to the β form as described earlier. By far, the crystal transform from α to β form is not well clarified. Takahashi *et al.*[31] and Sawai *et al.*[27] held the viewpoint that crystal transformation of PLLA took place between the $(0010)_\alpha$ reflection of α form and the $(003)_\beta$ reflection of β form. However, the observed strong diffraction peak at 2θ = 19.6º in the present study is consistent with the simulated β form diagram depicted by Brizzolara et al.[32] In addition, the diffraction intensity of β crystals with the EDR of 8.2 is stronger than that of the EDR of 6.3, providing evidence for the formation of higher amount of β crystals at higher EDR.

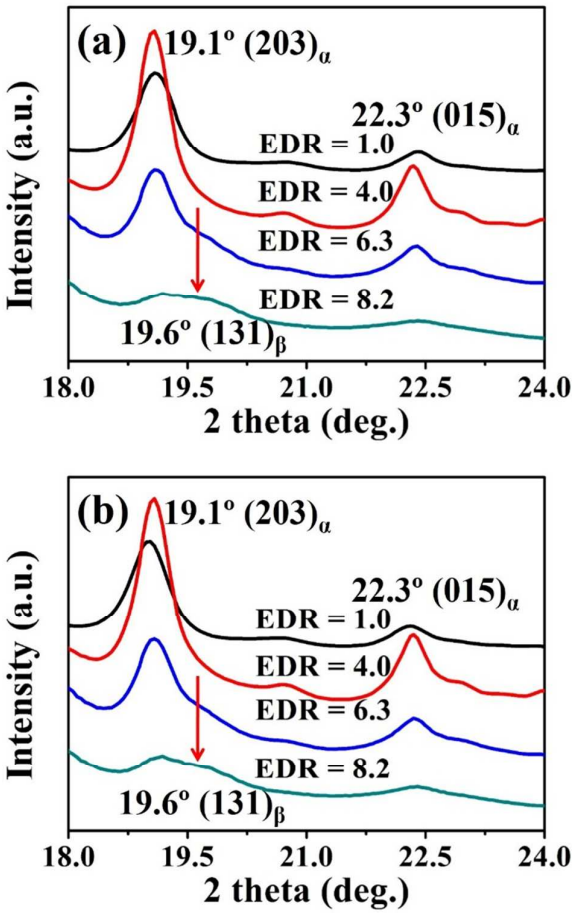

Fig. 6 Representative 1D-WAXD curves (2θ = 18° ~ 24°) of SSRE PLLA rods for different EDRs: (a) sheath, (b) core.

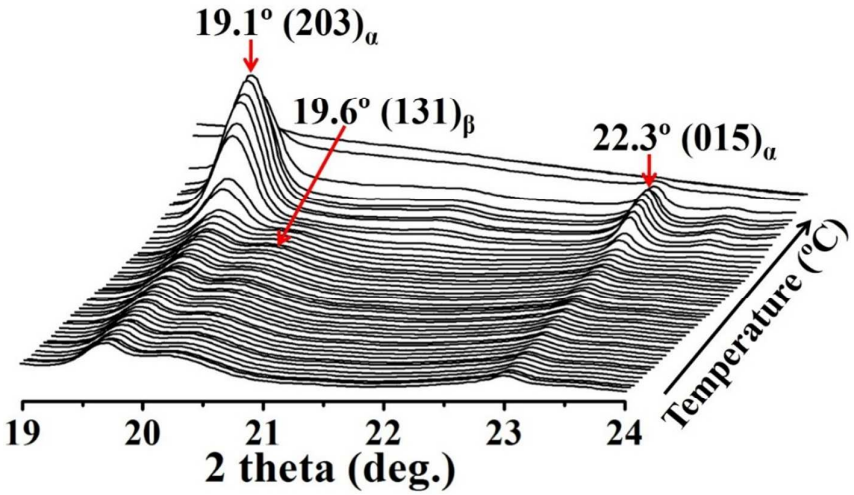

Fig. 7 Representative on-line 1D-WAXD curves (2θ =18° ~ 24°) of the sheath of SSRE PLLA rods with an EDR of 8.2.

With the purpose of revealing the structural disparities of α form and β form, on-line WAXD measurement was performed on the sheath of PLLA samples with the EDR of 8.2, where the β form is believed to be the most relative to the other parts in this study. The evolution of linear WAXD curves as a function of temperature is illustrated in Fig. 7. It could be observed that the $(131)_\beta$ reflection (2θ = 19.6º) of PLLA disappears first as the temperature increases, indicating that the β form is slightly less stable than the α form. The chains forced into an unfavorable arrangement by the strong flow field during SSRE, which mildly prevents the crystallization, might be a reason for this phenomenon.[19] On the other hand, the diffraction peaks of the $(203)_\alpha$ reflection (2θ = 19.1º) and the $(015)_\alpha$ reflection (2θ = 22.3º) of PLLA strengthens until the temperature reaches the melting point of α crystals, which corresponds to the perfecting process of α lamellae. It thus emphasizes that the crystal transformation from β form to α form during heating stems from the melting re-crystallization rather than the solid-solid phase transformation.

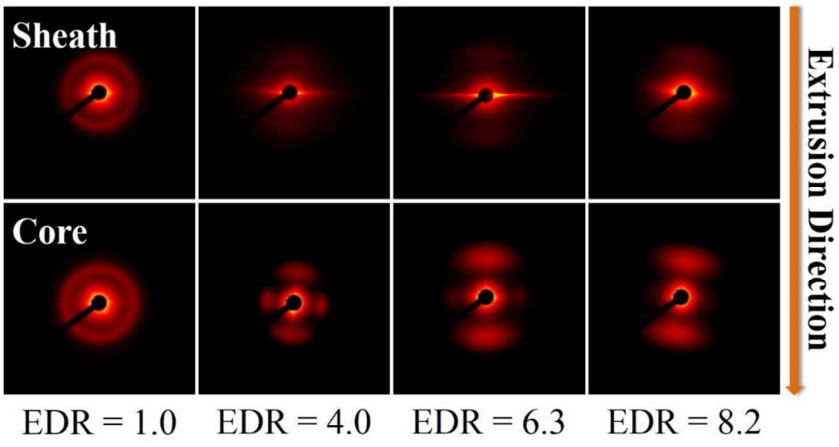

Fig. 8 Typical SAXS images of SSRE PLLA extrudates at different EDRs.

3.3 SAXS Analysis of the PLLA Extrudates

Fig. 8 depicts the typical SAXS patterns of PLLA samples at different EDRs to gain more convincing evidence of hierarchically structural information. At the EDR of 1.0, scattering pattern reveals an isotropic ring, implying that the lamellae in the PLLA billet are randomly distributed. As for the sheath, upon extrusion to high EDR, there are two symmetrical triangular streaks in the equatorial direction, which are the symbolic pattern of oriented fibrillar structure. It is intuitively confirmed that spherulites gradually transform into fibrils as the EDR increases. Meanwhile, it is also demonstrated that fibrillar structures are aligned along the extrusion direction, which is accordance with SEM and WAXD observations. The appearance of dumbbell-like scattering patterns in the meridional direction reflects the signal of the orientation of lamellae. Combining with SEM observation, it can be seen that the degree of orientation is strong in the sheath compared to the core. The more serious deformation occurred in the sheath of extruded rods could be the interpretation. Different from the WAXD result, the degree of orientation herein is comparable between the sheath and the core at high EDRs. It may be attributed to different detecting scales of the two characterization techniques.[33, 34]

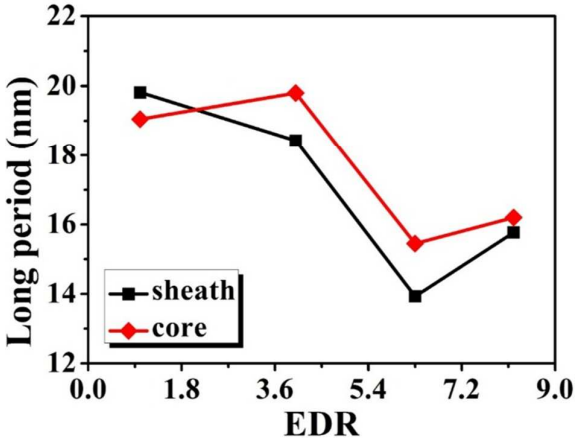

Fig. 9 The long period of the SSRE PLLA rods for different EDRs.

Long period of extruded PLLA in both sheath and core gradually falls down as the EDR increases from 1.0 to 6.3 (Fig. 9). The reduction of long period is probably a result of destruction of premier spherulites. As the EDR increases, the original lamellae may break into imperfect or defective lamellae, leading to the reduction of long period. Given the decreased melting enthalpy as shown in Table 1, we deduce that the lamellar thickness reduces gradually since the lamellar thickness reflects the product of long period and crystallinity. Nevertheless, the long period increases at the higher EDR, which mainly results from the destruction of the already formed defective crystals. Besides, the variation of long period in the core slightly lags behind that in the sheath. It is reasonable because the core has lower alteration extent of long period than the sheath. The different variation trend of long period between sheath and core is associated with the hierarchical deformation of SSRE PLLA.

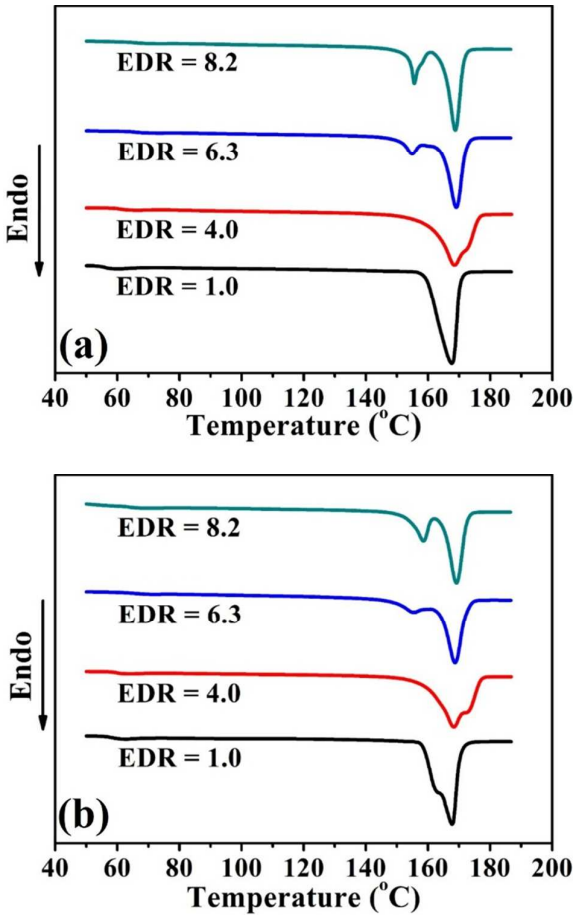

Fig. 10 DSC melting thermograms of SSRE PLLA rods for different EDRs: (a) sheath, (b) core.

3.4 Thermal Properties of the PLLA Extrudates

Fig. 10 shows DSC heating thermograms of the PLLA extrudates at different EDRs. It is found that a single melting peak (T_m) at 168 °C exists in the sheath at the EDR of 1.0, while double T_m are clearly observed at EDR above 4.0, showing that the α form transforms into the β form at the EDR of 6.3 and 8.2, which coincides with the report by Sawai.[27] The high T_m is due to the melting of α form, whereas the low T_m around 155 °C results from the melting of β form. When PLLA is extruded at the EDR of 4.0,

a shoulder T_m emerges in the DSC heating curve. The shoulder peak may derive from the formation of fibrous crystals. Moreover, with the increase of EDR, it could be detected that $X_{c\beta}$ is augmented as tabulated in Table 1, supporting that crystal transformation is more efficient by higher EDR. It should be noted that the melting process of α form emerges until the β form melts completely, indicating that the melting of SSRE PLLA containing the β crystals is related to the melting, re-crystallization and re-melting process in consistency with the description in Fig. 7. The T_m increases in both the sheath and the core (Table 1), which could be due to the formation of fibrous crystals and the melting re-crystallization. For the core, the variation trend is nearly the same as the sheath, but $X_{c\,\beta}$ in the core is lower against the sheath, which may be from the larger deformation in the sheath versus the core. Sawai *et al.*[27] explained this phenomenon was caused by the shear deformation, which might enhance the crystal transformation more effectively than the extensional deformation. Beyond that, we also find the width of T_m first broadens and then narrows with EDR. The former is due to deformation of the original spherulites, while the latter roots in the relatively uniform crystals forming with higher EDR. Meanwhile, because crystal fragmentation and distortion are more acute when the billet gets through a smaller convergent die with EDR, the ordered crystalline structure of polymer is destroyed, leading to lessening the absorbent heat of fusion. As a consequence, $X_{c\,\alpha}$ cuts down as shown in Table 1.

Table 1 T_m, ΔH_m and X_c of PLLA by SSRE

Region	EDR	$T_{m\beta}$ (°C)	$\Delta H_{m\beta}$ (J/g)	$X_{c\beta}$ (%)	$T_{m\alpha}$ (°C)	$\Delta H_{m\alpha}$ (J/g)	$X_{c\alpha}$ (%)
Sheath	1.0	—	—	—	167.65	60.36	64.42
	4.0	—	—	—	168.51	53.51	57.12
	6.3	154.83	3.65	2.94	169.13	33.47	35.72
	8.2	155.57	10.89	8.78	168.78	34.27	36.57
Core	1.0	—	—	—	167.72	58.96	62.92
	4.0	—	—	—	168.31	54.78	58.46
	6.3	155.03	2.17	1.75	168.73	30.74	32.81
	8.2	158.58	10.57	8.52	169.21	31.32	33.43

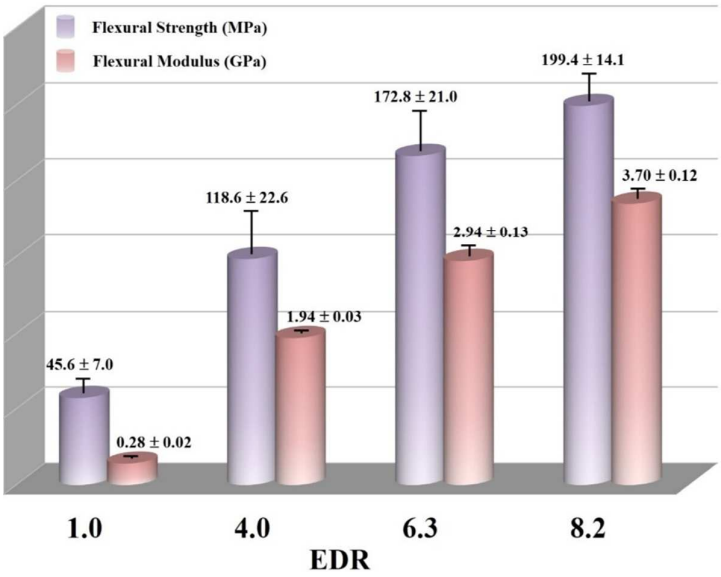

Fig. 11 Flexural strength and flexural modulus of SSRE PLLA rods for different EDRs.

3.5 Mechanical Properties of the SSRE PLLA Extrudates

Flexural property of SSRE PLLA as a function of EDR is illustrated in Fig. 11. The SSRE PLLA extrudates show monotonous rise in both flexural strength and flexural modulus with EDR. The flexural strength increases by about 400%, from 45.6 MPa for the sample at the EDR of 1.0 up to 199.4 MPa for the sample at the EDR of 8.2. Similar enhancement was observed in terms of flexural modulus, which rises from 0.28 GPa to 3.70 GPa. Such an escalation of flexural properties is owing to the high orientation of molecular chains and the formation of microfibrillar reinforcement structure, as verified by SEM observation, WAXD and SAXS measurements.

By means of the SSRE technique, we prepared the PLLA extrudates with self-reinforcement structure, where the primal spherulites transformed into robust microfibers aligned along the extrusion direction, enhancing the flexural strength and modulus drastically. The value of flexural strength for SSRE PLLA could meet target requirement of cancellous bone (~ 20 MPa), and is even comparable to that of cortical bone (~ 200 MPa).[35] The SSRE PLLA is believed to offer potential biomedical applications in bone fixation devices, such as bone plates, screws, and so on.

4. Conclusions

The bulk PLLA was successfully extruded by the home-made SSRE apparatus. Effects of EDRs on the morphology, structure, thermal properties, and mechanical properties of the SSRE PLLA rods were systemically investigated by SEM, WAXD, SAXS, DSC and three point flexural test. The initial spherulites gradually transformed into fibers along the extrusion direction. Due to the intense flow fields in the die,

molecular chains were compelled to align along the flow direction. Intriguingly, the crystal transformation from the initial α form to the β form which occurred between $(203)_\alpha$ and $(131)_\beta$ was detected with the increase of EDR. At the meantime, it proceeded more rapidly in the sheath region than the core region. DSC results confirmed a mixture of α and β crystals in SSRE PLLA, which showed the melting temperature at 168 and 155 °C, respectively. And the multiple melting process of SSRE PLLA was unfolded to be the melting re-crystallization and re-melting process. The increased melting point derived from the contribution of fibrous crystals and melting re-crystallization. Compared to the sample at the EDR of 1.0, flexural strength and flexural modulus showed 4 times and 13 times higher for the specimen at the EDR of 8.2, respectively. The SSRE technique offered a feasible way to improve the mechanical properties of PLLA.

Acknowledgements

The authors gratefully acknowledge the financial support from the Program of National Natural Science of China (51120135002, 51421061), Sichuan Youth Science and Technology Innovation Research Team (2014TD0002), the Specialized Research Fund for the Doctoral Program of Higher Education (20130181130012) and Outstanding Youth Talent Program of State Key Laboratory of Polymer Materials Engineering (sklpme2014-3-08). We would like to express sincere thanks to the Shanghai Synchrotron Radiation Facility (SSRF, Shanghai, China) for the kind help on WAXD and SAXS measurements.

References

1 W. Amass, A. Amass and B. Tighe, *Polym. Int.*, 1998, **47**, 89-144.

2 A. G. Coombes and M. C. Meikle, *Clin. Mater.*, 1994, **17**, 35-67.

3 Y. Ikada, *Adv. Eng. Mater.*, 1999, **1**, 67-68.

4 M. Martina and D. W. Hutmacher, *Polym. Int.*, 2007, **56**, 145-157.

5 M. I. Sabir, X. Xu and L. Li, *J. Mater. Sci.*, 2009, **44**, 5713-5724.

6 J. B. Zeng, K. A. Li and A. K. Du, *RSC Adv.*, 2015, **5**, 32546-32565.

7 Y. Ikada and H. Tsuji, *Macromol. Rapid Commun.*, 2000, **21**, 117-132.

8 H. Okuzaki, I. Kubota and T. Kunugi, *J. Polym. Sci., Part B: Polym. Phys.*, 1999, **37**, 991-996.

9 B. Eling, S. Gogolewski and A. Pennings, *Polymer*, 1982, **23**, 1587-1593.

10 B. Kalb and A. Pennings, *Polymer*, 1980, **21**, 607-612.

11 T. Miyata and T. Masuko, *Polymer*, 1997, **38**, 4003-4009.

12 J. Q. Li, P. T. Xiao, H. F. Li, Y. Zhang, F. F. Xue, B. J. Luo, S. Y. Huang, Y. R. Shang, H. Y. Wen, J. D. C. Christiansen, D. H. Yu and S. C. Jiang, *Polym. Chem.*, 2015, **6**, 3988-4002.

13 Z. B. Qiu and P. Zhou, *RSC Adv.*, 2014, **4**, 51411-51417.

14 Q. X. Liu, R. H. Lv, B. Na and Y. H. Ju, *RSC Adv.*, 2015, **5**, 57076-57081.

15 J. Puiggali, Y. Ikada, H. Tsuji, L. Cartier, T. Okihara and B. Lotz, *Polymer*, 2000, **41**, 8921-8930.

16 L. Cartier, T. Okihara, Y. Ikada, H. Tsuji, J. Puiggali and B. Lotz, *Polymer*, 2000, **41**, 8909-8919.

17 J. M. Zhang, Y. X. Duan, H. Sato, H. Tsuji, I. Noda, S. Yan and Y. Ozaki, *Macromolecules*, 2005, **38**, 8012-8021.

18 J. W. Leenslag and A. J. Pennings, *Polymer*, 1987, **28**, 1695-1702.

19 W. Hoogsteen, A. Postema, A. Pennings, G. Ten Brinke and P. Zugenmaier, *Macromolecules*, 1990, **23**, 634-642.

20 P. D. Coates, A. G. Gibson and I. M. Ward, *J. Mater. Sci.*, 1980, **15**, 359-375.

21 C. J. Farrell and A. Keller, *J. Mater. Sci.*, 1977, **12**, 966-974.

22 K. Imada, T. Yamamoto, K. Shigematsu and M. Takayanagi, *J. Mater. Sci.*, 1971, **6**, 537-546.

23 W. G. Perkins and R. S. Porter, *J. Mater. Sci.*, 1977, **12**, 2355-2388.

24 A. E. Zachariades, W. Mead and R. S. Porter, *Chem. Rev.*, 1980, **80**, 351-364.

25 Y. B. Li, *J. Macromol. Sci., Part B: Phys.*, 2009, **48**, 344-350.

26 S. Ferguson, D. Wahl and S. Gogolewski, *J. Biomed. Mater. Res.*, 1996, **30**, 543-551.

27 D. Sawai, K. Takahashi, T. Imamura, K. Nakamura, T. Kanamoto and S. H. Hyon, *J. Polym. Sci., Part B: Polym. Phys.*, 2002, **40**, 95-104.

28 D. Sawai, K. Takahashi, A. Sasashige, T. Kanamoto and S. H. Hyon, *Macromolecules*, 2003, **36**, 3601-3605.

29 D. Sawai, T. Yokoyama, T. Kanamoto, M. Sungil, S. H. Hyon and L. P. Myasnikova, *Macromol. Symp.*, 2006, **242**, 93-103.

30 H. Xu, C. Y. Liu, C. Chen, B. S. Hsiao, G. J. Zhong and Z. M. Li, *Biopolymers*, 2012, **97**, 825-839.

31 K. Takahashi, D. Sawai, T. Yokoyama, T. Kanamoto and S. H. Hyon, *Polymer*, 2004, **45**, 4969-4976.

32 D. Brizzolara, H. J. Cantow, K. Diederichs, E. Keller and A. J. Domb, *Macromolecules*, 1996, **29**, 191-197.

33 R. H. Somani, L. Yang, B. S. Hsiao, P. K. Agarwal, H. A. Fruitwala and A. H. Tsou,

Macromolecules, 2002, **35**, 9096-9104.

34 Z. G. Wang, B. S. Hsiao, E. B. Sirota, P. Agarwal and S. Srinivas, *Macromolecules*, 2000, **33**, 978-989.

35 J. Y. Lim, S. H. Kim, S. Lim and Y. H. Kim, *Macromol. Chem. Phys.*, 2001, **202**, 2447-2453.

Effects of extrusion draw ratio on morphology, structure and mechanical properties of poly(L-lactic acid) fabricated by solid state ram extrusion

Hua-Mo Yin, Huan Xu, Jin Zhang, Jing-Bin Chen, Jun Lei, Jia-Zhuang Xu* and Zhong-Ming Li*

College of Polymer Science and Engineering and State Key Laboratory of Polymer Materials Engineering, Sichuan University, Chengdu 610065, China

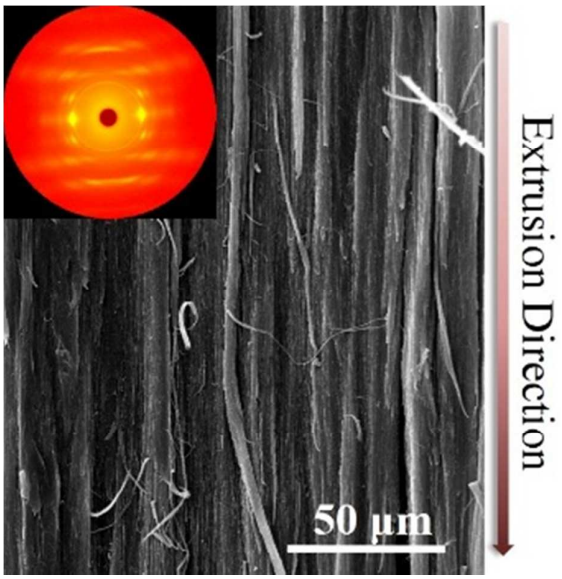

The utilization of SSRE technique induced highly oriented PLLA.

*Corresponding author. Tel.: +86-28-8540-0211; Fax: +86-28-8540-5402; E-mail address: zmli@scu.edu.cn (Z.M. Li); E-mail address: jzxu@scu.edu.cn (J.Z. Xu)